

COVER PAGE

Document downloaded by @DAEL

Thu Nov 26 21:47:16 2026
For personal use

When automatic English translation is provided, only the original document is authentic.
The EAA cannot be held responsible of any translation error

Bibliographical reference

Statistical Characterization of Sound Propagation Over Vertical and Slanted Paths in a Turbulent Atmosphere, Vladimir E. Ostashev and D. Keith Wilson, Acta Acustica **vol. 104** (Number 4), 2018, pp. 571-585

DOI
https://doi.org/10.3813/AAA.919198

Acta Acustica united with Acustica
Vol. 104 (2018) 571 – 585

DOI 10.3813/AAA.919198

Statistical Characterization of Sound Propagation Over Vertical and Slanted Paths in a Turbulent Atmosphere

Vladimir E. Ostashev, D. Keith Wilson
U.S. Army Engineer Research and Development Center, 72 Lyme Rd., Hanover, NH 03755, U.S.A.
vladimir.ostashev@colorado.edu

Summary
Most previous research on sound propagation in the turbulent atmosphere has focused on nearly horizontal propagation. Sound propagation over vertical and slanted paths is fundamentally different from horizontal propagation in that the variances and length scales of the turbulence depend on the height above the ground. In this paper, propagation over vertical and slanted paths is studied using approaches and methods developed for wave propagation through inhomogeneous, random media. Statistical characteristics of sound signals such as the extinction coefficient of the mean sound field, the strength parameter, the transverse mutual coherence function, the coherence radius, and the correlation functions and variances of the phase and log-amplitude fluctuations are calculated for arbitrary spectra of temperature and wind velocity fluctuations, and then specialized to the von Kármán model for the turbulence spectra. The extinction coefficient and coherence radius are analyzed numerically for various meteorological conditions of the atmospheric boundary layer. The results obtained are compared with those for near-horizontal sound propagation. The theory has applications to localization of elevated sound sources with ground-based microphone arrays, and the detection of ground-based sources with elevated arrays.

PACS no. 43.28.-g

1. Introduction

Most previous research on sound propagation in the atmosphere has focused on nearly horizontal propagation paths, with the sources and receivers close to the ground [1]. Many significant advances have been made during the last several decades regarding theoretical treatments of sound propagation through atmospheric turbulence (see [2] and references therein). In particular, more realistic turbulence models have become available, and scattering theories have advanced to address phenomena such as the phase and log-amplitude fluctuations of acoustic signals and their spatial, temporal, and frequency coherence [3].

Sound propagation from elevated sources is fundamentally different from horizontal propagation in that the variances and length scales of temperature and wind velocity fluctuations depend significantly on the height above the ground. The vertical and slanted sound propagation have been studied to a much lesser extent. Improved understanding of this problem is essential to predicting the ability of ground-based acoustic beamforming array systems (acoustic "antennas") to detect and track elevated sound sources, as well as the ability of elevated arrays to detect and localize ground-based sources. The research is timely in its applicability to a large number of current problems such as tracking small unattended aerial systems (UASs) and assessing the effect of atmospheric turbulence on sonic booms. This paper studies the effect of temperature and wind velocity fluctuations on the statistical characteristics of sound signals for vertical and slanted propagation.

Parkin and Scholes [4, 5] were apparently the first to publish measurements of sound levels from low-flying aircraft. Their first experiment involved a small commuter airplane at an altitude up to 610 m, for the purpose of quantifying atmospheric sound attenuation along near-vertical paths. Their second experiment dealt with helicopters at altitudes up to 305 m, with a focus on attenuation along oblique, nearly horizontal paths. Aubry et al. [6] performed what was, at the time, a highly innovative experiment involving microphones on a tethered balloon at an altitude of 900 m. The focus was on measuring the attenuation in excess of molecular attenuation, namely due to scattering by turbulence, which at the time was a poorly understood concept. Shortly after the work of Aubry et al. a feasibility study was conducted on the use of a meteorological tower for air-to-ground sound propagation [7]. An acoustic source mounted 150 m above ground was aimed along a guy wire fitted with an array of microphones. Due to the slow response of the meteorological sensors available for this study, the fluctuations in sound pressure amplitude and phase could not be related to the

Received 4 January 2018,
accepted 30 April 2018.

© S. Hirzel Verlag · EAA

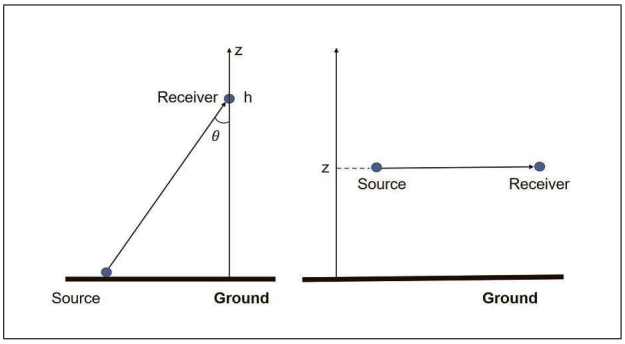

Figure 1. Geometries of sound propagation in the atmosphere. (Left) Slanted propagation from the source on the ground to the elevated receiver, and (right) horizontal propagation parallel to the ground.

atmospheric turbulence. More recent measurements have also been performed with elevated sources, although the maximum height was only 30 m (the maximum height of the tower available), and thus the propagation path was still nearly horizontal [8, 9, 10].

Research on sonic boom propagation is a notable exception to the typical emphasis on near-horizontal paths. This problem has generated renewed interest due to prospects for building new commercial supersonic aircraft with reduced shock footprints [11]. Since such aircraft fly at a much higher altitude than small UASs and helicopters, most of the propagation path is in the stratosphere and free troposphere, although significant scattering in the atmospheric boundary layer (ABL) does occur and researchers have attempted to model this phenomenon (e.g., [12, 13, 14, 15]). Auralization of flying aircraft is another problem where statistical characteristics of sound signals over slanted paths in a turbulent atmosphere are needed [16, 17].

A general theory of sound propagation through an inhomogeneous atmospheric turbulence is summarized in [2]. Here we employ that theory to calculate the statistical characteristics of sound signals propagating over vertical and slanted paths in a turbulent atmosphere, in which the variances and length scales of temperature and wind velocity fluctuations depend on the height above the ground. The theory utilizes on a realistic, general model for the variances and length scales of turbulence in the ABL.

This paper examines the following statistical characteristics of sound signals: the extinction coefficient of the mean sound field, the strength parameter, the transverse mutual coherence function, the coherence radius, and the correlation functions and variances of the phase and log-amplitude fluctuations. Brief descriptions of these statistical characteristics are provided; more detailed formulations can be found in the literature (e.g., [2, 18]). Two geometries of sound propagation are considered: a ground-based source and an elevated receiver, and an elevated source and ground-based receiver. Formulations for the statistical characteristics are provided for arbitrary spectra of temperature and wind velocity fluctuations and then more results are specifically derived for the generalized von Kármán spectra. The extinction coefficient and the coherence radius are calculated for various meteorological conditions of the ABL characterized by the surface heat flux and friction velocity. These results are compared with those for horizontal sound propagation.

The paper is organized as follows. Section 2 presents formulation of the problem and the turbulence model. The extinction coefficient for vertical and slanted sound propagation is studied in Section 3. Section 4 considers the strength parameter. In Section 5, the spatial coherence of acoustic signals is analyzed. The correlation functions and variances of the phase and log-amplitude fluctuations are considered in Section 6. The results are summarized in Section 7.

2. Formulation of the problem and turbulence model

2.1. Formulation of the problem

The geometry of slanted sound propagation is shown in the left plot in Figure 1. The z axis is perpendicular to the ground. The source is located on the ground and the receiver (a microphone array) is well above the ground, at the height h. The propagation angle between the path and the z axis is θ. The length of the propagation path is $L = h/\cos\theta$.

We will also consider the case when the sound source is well above the ground, while the receiver is on the ground. In this case, the geometry of the problem is still given by Figure 1, if the positions of the source and receiver are switched.

In this paper, we will calculate and analyze the statistical characteristics of sound signals for slanted propagation ($\theta \neq 0$) and vertical propagation ($\theta = 0$). These statistical characteristics will be compared with those for horizontal sound propagation at the height z above the ground, as shown in the right plot in Figure 1.

The statistical moments of the sound field depend on the temperature and wind velocity fluctuations along the propagation path. In this paper, these statistical moments are derived for arbitrary spectra of statistically isotropic temperature and wind velocity fluctuations, $\tilde{\Phi}_T(z, \kappa)$ and $E(z, \kappa)$, and then specified for the generalized von Kármán spectra. Here, κ is the turbulence wavenumber. Following [2, 18], the remaining part of this section outlines the most advanced turbulence model currently used in atmospheric acoustics.

2.2. Generalized von Kármán spectra

The generalized von Kármán spectra extend the ordinary von Kármán spectra to cases where the inertial subrange does not have the classic Kolmogorov decay. This may occur, for example, if the turbulence is intermittent. For temperature and wind velocity fluctuations, the generalized von Kármán spectra are given in [18],

$$\tilde{\Phi}_T(z;\kappa) = \frac{\Gamma(\alpha)}{\pi^{3/2}\Gamma(\alpha - 3/2)} \frac{\sigma_T^2(z)\, L_T^3(z)}{\left(1 + \kappa^2 L_T^2(z)\right)^{\alpha}}, \quad (1)$$

$$E(z;\kappa) = \frac{4\alpha\Gamma(\alpha)}{\sqrt{\pi}\Gamma(\alpha-3/2)} \frac{\sigma_v^2(z)\, L_v^5(z)\, \kappa^4}{\left(1+\kappa^2 L_v^2(z)\right)^{\alpha+1}}. \quad (2)$$

Here, α is a parameter ($\alpha > 3/2$), Γ is the gamma function, σ_T^2 and σ_v^2 are the variances of temperature and wind velocity fluctuations, and L_T and L_v are the corresponding length scales.

The ordinary von Kármán spectra are obtained by setting $\alpha = 11/6$ in Equations (1) and (2); they coincide with the Kolmogorov spectra for large κ. The case $\alpha \neq 11/6$ corresponds to non-Kolmogorov turbulence which occurs in several applications (e.g., in turbulent flows with local and global intermittency [20]) and has been employed in optical communication systems [21, 22].

In what follows, we will also use the integral length scales of temperature and velocity fluctuations, $\mathcal{L}_T$ and $\mathcal{L}_v$, defined as follows (e.g., [2, 18, 19]):

$$\begin{aligned}\mathcal{L}_T(z) &= \frac{1}{\sigma_T^2(z)} \int_0^\infty B_T(z;R)\, \mathrm{d}R \\ &= \frac{2\pi^2}{\sigma_T^2(z)} \int_0^\infty \tilde{\Phi}_T(z;\kappa)\kappa\, \mathrm{d}\kappa, \quad (3)\\ \mathcal{L}_v(z) &= \frac{1}{\sigma_v^2(z)} \int_0^\infty B_{11}(z;R)\, \mathrm{d}R \\ &= \frac{\pi}{2\sigma_v^2(z)} \int_0^\infty \frac{E(z;\kappa)}{\kappa}\, \mathrm{d}\kappa. \quad (4)\end{aligned}$$

Here, $B_T(z;R)$ and $B_{11}(z;R)$ are the correlation functions of the temperature and longitudinal velocity fluctuations. These formulas are valid for arbitrary spectra of turbulence. For the generalized von Kármán spectra, the integral length scales can be expressed in terms of L_T and L_v [18, 19],

$$\mathcal{L}_T(z) = \frac{\sqrt{\pi}\Gamma(\alpha-1)}{\Gamma(\alpha-3/2)} L_T(z), \quad (5)$$

$$\mathcal{L}_v(z) = \frac{\sqrt{\pi}\Gamma(\alpha-1)}{\Gamma(\alpha-3/2)} L_v(z). \quad (6)$$

2.3. Height dependence of the variances and length scales

The dependence of the variances, σ_T^2 and σ_v^2, and the length scales, L_T and L_v, on the height above the ground is outlined in Section 6.2.4 of [2]. For both shear- and buoyancy-produced turbulence, σ_T^2 and L_T are given by,

$$\sigma_T^2(z) = \frac{4.0\, T_*^2}{(1-10z/L_o)^{2/3}}, \quad (7)$$

$$L_T(z) = 2.0\, z \frac{(1-7z/L_o)}{(1-10z/L_o)}, \quad (8)$$

where $T_* = -\Gamma_d Q_H/(g\varrho_a u_*)$ is a temperature scale and $L_o = -u_*^3 T_r \varrho_a/(\kappa_v \Gamma_d Q_H)$ is the Monin-Obukhov length. Here u_* is the friction velocity, Q_H is the surface heat flux, T_r is the reference temperature at the height z_r, $\kappa_v = 0.40$ is the von Kármán constant, g is the gravitational acceleration, ϱ_a is the air density, and $\Gamma_d = 0.0098$ K/m is the dry adiabatic lapse rate.

The values of σ_v^2 and L_v for shear-produced turbulence are given by

$$\sigma_{v,s}^2 = 3.0\, u_*^2, \quad L_{v,s}(z) = 1.8\, z, \quad (9)$$

and for buoyancy-produced turbulence

$$\sigma_{v,b}^2 = 0.35\, w_*^2, \quad L_{v,b} = 0.23\, z_i. \quad (10)$$

Here, z_i is the boundary layer inversion height and $w_* = \left[z_i \Gamma_d Q_H/(\varrho_a T_r)\right]^{1/3}$ is the convection velocity scale. The subscripts v,s and v,b stand for shear-produced and buoyancy-produced velocity fluctuations, respectively. When both shear and buoyancy forcings are present, the corresponding energy spectra $E(\kappa)$ should be summed.

In this paper, we assume that $Q_H \geq 0$ so that $1/L_o \leq 0$; this corresponds to unstable and neutral stratifications, which usually occur during daytime. In stable conditions ($Q_H < 0$), which usually occur at night, turbulence tends to be suppressed.

3. Extinction coefficient

In the turbulent atmosphere, the mean of the complex sound pressure field decays exponentially. The rate of the decay is termed as the extinction coefficient of the mean field, which plays an important role in the theories of wave propagation in random media.

3.1. Horizontal propagation

This subsection summarizes the results pertinent to the extinction coefficient for horizontal propagation [2, 18].

For sound propagation in the turbulent atmosphere, the mean sound field is given by

$$\langle p \rangle = p_0 \exp\left(-x\gamma\right). \quad (11)$$

Here, the brackets $\langle\ \rangle$ indicate averaging over an ensemble of realizations of temperature and velocity fluctuations, p_0 is the sound field in a non-turbulent atmosphere, x is the propagation range, and $\gamma(z)$ is the extinction coefficient for horizontal propagation at the height z above the ground (Figure 1). The extinction coefficient is given by (Equation (7.153) in [2]),

$$\gamma(z) = \frac{\pi^2 k^2}{2} \int_0^\infty \Phi_{\mathrm{eff}}(z;\kappa)\kappa\, \mathrm{d}\kappa. \quad (12)$$

In this formula, k is the sound wavenumber and Φ_{eff} is the effective spectrum of turbulence, which depends on the height z above the ground,

$$\Phi_{\mathrm{eff}}(z;\kappa) = \frac{\tilde{\Phi}_T(z;\kappa)}{T_0^2} + \frac{E(z;\kappa)}{\pi c_0^2 \kappa^2}, \quad (13)$$

where T_0 and c_0 are the reference values of temperature and sound speed. Substituting the effective spectrum into Equation (12), the extinction coefficient can be expressed as

$$\gamma(z) = \gamma_T(z) + \gamma_v(z). \tag{14}$$

Here, $\gamma_T(z)$ and $\gamma_v(z)$ are the contributions to the extinction coefficient due to temperature and velocity fluctuations, respectively,

$$\gamma_T(z) = \frac{\pi^2 k^2}{2T_0^2}\int_0^\infty \tilde{\Phi}_T(z;\kappa)\kappa\,\mathrm{d}\kappa = \frac{k^2\sigma_T^2(z)\mathcal{L}_T(z)}{4T_0^2}, \tag{15}$$

$$\gamma_v(z) = \frac{\pi k^2}{2c_0^2}\int_0^\infty \frac{E(z;\kappa)}{\kappa}\,\mathrm{d}\kappa = \frac{k^2\sigma_v^2(z)\mathcal{L}_v(z)}{c_0^2}. \tag{16}$$

In these formulas, using Equations (3) and (4), the integrals over κ were expressed in terms of $\sigma_T^2\mathcal{L}_T$ and $\sigma_v^2\mathcal{L}_v$, respectively.

This formulation for the extinction coefficient is valid for arbitrary spectra of turbulence. Substitution of the integral length scales $\mathcal{L}_T$ and $\mathcal{L}_v$ given by Equations (5) and (6) into Equations (15) and (16) yields the temperature and velocity contributions to the extinction coefficient $\gamma(z)$ for the generalized von Kármán spectra,

$$\gamma_T(z) = \frac{\sqrt{\pi}\Gamma(\alpha-1)}{\Gamma(\alpha-3/2)}\frac{k^2\sigma_T^2(z)L_T(z)}{4T_0^2}, \tag{17}$$

$$\gamma_v(z) = \frac{\sqrt{\pi}\Gamma(\alpha-1)}{\Gamma(\alpha-3/2)}\frac{k^2\sigma_v^2(z)L_v(z)}{c_0^2}. \tag{18}$$

Taking into account that the wind velocity fluctuations are due to shear and buoyancy, the extinction coefficient can be written as

$$\gamma(z) = \gamma_T(z) + \gamma_{v,s}(z) + \gamma_{v,b}. \tag{19}$$

The extinction coefficient due to temperature fluctuations is obtained with the use of Equations (7), (8), and (17),

$$\gamma_T(z) = \frac{\sqrt{\pi}\Gamma(\alpha-1)}{5\Gamma(\alpha-3/2)}\frac{k^2T_*^2(-L_o)}{T_0^2}F_{\mathrm{hor}}\left(\frac{10z}{-L_o}\right). \tag{20}$$

The function F_{hor} characterizes the dependence of γ_T on the normalized height $\xi = 10z/(-L_o)$ above the ground,

$$F_{\mathrm{hor}}(\xi) = \xi\frac{1+0.7\xi}{(1+\xi)^{5/3}}. \tag{21}$$

It follows from this equation that $F_{\mathrm{hor}} \approx \xi$ for small ξ and $F_{\mathrm{hor}} \approx 0.7\xi^{1/3}$ for $\xi \gg 1$. The function $F_{\mathrm{hor}}(\xi)$ is plotted in Figure 2.

The extinction coefficient $\gamma_{v,s}$ is obtained with Equations (9) and (18),

$$\gamma_{v,s}(z) = \frac{5.4\sqrt{\pi}\Gamma(\alpha-1)}{\Gamma(\alpha-3/2)}\frac{k^2u_*^2}{c_0^2}z. \tag{22}$$

This extinction coefficient increases linearly with height.

Finally, the extinction coefficient $\gamma_{v,b}$ is obtained with Equations (10) and (18),

$$\gamma_{v,b} = \frac{0.0805\sqrt{\pi}\Gamma(\alpha-1)}{\Gamma(\alpha-3/2)}\frac{k^2w_*^2}{c_0^2}z_i. \tag{23}$$

The extinction coefficient $\gamma_{v,b}$ does not depend on height.

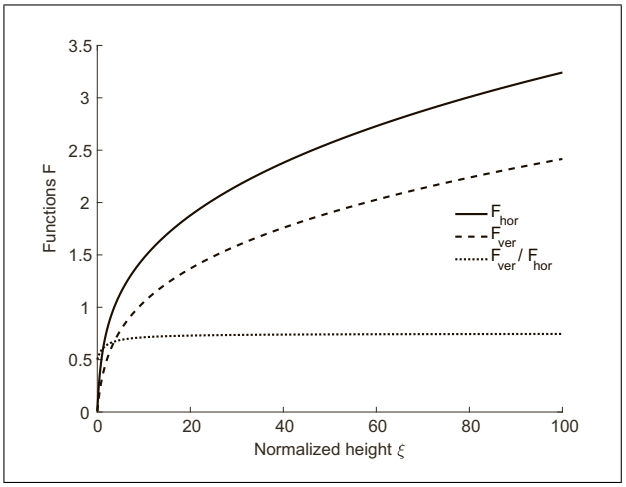

Figure 2. Functions F_{hor} and F_{ver} pertinent to horizontal and vertical sound propagation versus the normalized height above the ground ξ. For horizontal propagation, $\xi = 10z/(-L_o)$, and for vertical propagation, $\xi = 10h/(-L_o)$.

3.2. Slanted propagation

For slanted propagation from the ground-based source to the elevated receiver (Figure 1), the mean sound field is given by Equations (7.150) and (7.151) in [2],

$$\langle p\rangle = p_0\exp\left(-L\bar{\gamma}\right) = p_0\exp\left(-\frac{h\bar{\gamma}}{\cos\theta}\right). \tag{24}$$

Here, $\bar{\gamma}$ is the extinction coefficient for slanted propagation. For isotropic turbulence,

$$\bar{\gamma} = \frac{\pi^2k^2}{2L}\int_0^L \mathrm{d}l\int_0^\infty \Phi_{\mathrm{eff}}(l\cos\theta;\kappa)\kappa\,\mathrm{d}\kappa, \tag{25}$$

where l is the integration variable along the sound propagation path from the source ($l = 0$) to the receiver ($l = L$). In Equation (25), we took into account that the effective spectrum depends on the height $z = l\cos\theta$ of the point on the propagation path. Introducing the new integration variable $z = l\cos\theta$, we have

$$\bar{\gamma}(h) = \frac{1}{h}\int_0^h \mathrm{d}z\int_0^\infty \frac{\pi^2k^2}{2}\Phi_{\mathrm{eff}}(z;\kappa)\kappa\,\mathrm{d}\kappa. \tag{26}$$

Comparison of this formula with Equation (12) yields

$$\bar{\gamma}(h) = \frac{1}{h}\int_0^h \gamma(z)\,\mathrm{d}z. \tag{27}$$

Equation (27) is a new result obtained in the paper. It follows from this equation that the extinction coefficient $\bar{\gamma}(h)$ for slanted propagation from the ground-based source to the elevated receiver is equal to the height-averaged extinction coefficient for horizontal propagation $\gamma(z)$. Since $\bar{\gamma}(h)$ does not depend on the propagation angle θ, the extinction coefficient for slanted propagation coincides with that for vertical propagation. According to Equation (24), the mean sound field for a slanted path differs from that for a vertical path only by the factor $1/\cos\theta$.

If the variances and length scales of temperature and wind velocity fluctuations do not depend on z, the extinction coefficient γ also does not depend on z and, according to Equation (27), $\bar{\gamma} = \gamma$. In other words, in this case, the extinction coefficients for horizontal and vertical propagation coincide as they should.

Equation (27) can be readily generalized to the case when the source is located at the height z_s above the ground,

$$\bar{\gamma}(h) = \frac{1}{h - z_s} \int_{z_s}^{h} \gamma(z)\, \mathrm{d}z. \tag{28}$$

In this case, the mean sound field is still given by Equation (24) if h is replaced with $h - z_s$. It can be shown from Equations (24) and (28) that if $z_s \to h$ and $\theta \to 0$, the mean sound field and the extinction coefficient for slanted propagation become those for horizontal propagation.

For slanted propagation from the elevated source to the ground-based receiver, the mean sound field is still given by Equation (24). The extinction coefficient is determined with Equation (25), where l is the integration variable along the propagation path from the elevated source ($l = 0$) to the ground-based receiver ($l = L$) and $\Phi_{\text{eff}} = \Phi_{\text{eff}}((L - l)\cos\theta; \kappa)$; here $z = (L - l)\cos\theta$ is the height of the point on the path. Introducing the new integration variable $z = (L - l)\cos\theta$, it can be shown that this extinction coefficient is given by Equation (26). Thus, if positions of the source and receiver are switched in Figure 1, the mean sound field and the extinction coefficient are still given by Equations (24) and (27). In other words, for the mean field, sound propagation is reciprocal.

Substituting with Equation (14), the extinction coefficient $\bar{\gamma}$ can be expressed as a sum of the contributions due to temperature and velocity fluctuations, $\bar{\gamma}_T$ and $\bar{\gamma}_v$, respectively,

$$\bar{\gamma}(h) = \bar{\gamma}_T(h) + \bar{\gamma}_v(h), \tag{29}$$

where

$$\bar{\gamma}_T(h) = \frac{1}{h} \int_0^h \gamma_T(z)\, \mathrm{d}z, \quad \bar{\gamma}_v(h) = \frac{1}{h} \int_0^h \gamma_v(z)\, \mathrm{d}z. \tag{30}$$

For the generalized von Kármán spectra, $\bar{\gamma}_T$ and $\bar{\gamma}_v$ are obtained by substituting Equations (20), (22), and (23) into Equation (30) and evaluating the integrals over z. The resulting extinction coefficient is a sum of three terms,

$$\bar{\gamma}(h) = \bar{\gamma}_T(h) + \bar{\gamma}_{v,s}(h) + \bar{\gamma}_{v,b}. \tag{31}$$

Here,

$$\bar{\gamma}_T(h) = \frac{\sqrt{\pi}\,\Gamma(\alpha - 1)}{5\Gamma(\alpha - 3/2)} \frac{k^2 T_*^2 (-L_o)}{T_0^2} F_{\text{ver}}\left(\frac{10h}{-L_o}\right). \tag{32}$$

The function F_{ver} characterizes the dependence of $\bar{\gamma}_T$ on the normalized height $\xi = 10h/(-L_o)$ of the receiver,

$$\begin{aligned} F_{\text{ver}}(\xi) &= \frac{1}{\xi} \int_0^{\xi} F_{\text{hor}}(\xi_1)\, \mathrm{d}\xi_1 \\ &= \xi^{-1} \left[0.225 + 0.525(1 + \xi)^{4/3} \right. \\ &\quad \left. - 1.2(1 + \xi)^{1/3} + 0.45(1 + \xi)^{-2/3}\right]. \end{aligned} \tag{33}$$

It can be shown from this formula that $F_{\text{ver}} \approx \xi/2$ for small ξ and $F_{\text{ver}} \approx 0.525\,\xi^{1/3}$ for $\xi \gg 1$. The function $F_{\text{ver}}(\xi)$ is plotted in Figure 2. The figure also depicts the ratio $F_{\text{ver}}(\xi)/F_{\text{hor}}(\xi)$ which monotonically increases from 0.5 to 0.75.

The extinction coefficient $\bar{\gamma}_{v,s}(h)$ is given by

$$\bar{\gamma}_{v,s}(h) = \frac{5.4\sqrt{\pi}\,\Gamma(\alpha - 1)}{\Gamma(\alpha - 3/2)} \frac{k^2 u_*^2}{c_0^2} \frac{h}{2}. \tag{34}$$

This extinction coefficient increases linearly with the height h of the receiver. Comparing this formula with Equation (22), we obtain

$$\bar{\gamma}_{v,s}(h) = \gamma_{v,s}(h/2). \tag{35}$$

This formula relates the extinction coefficients for vertical and horizontal propagation.

Finally, since the extinction coefficient $\gamma_{v,b}$ does not depend on the height z, we have

$$\bar{\gamma}_{v,b} = \gamma_{v,b}. \tag{36}$$

For the generalized von Kármán spectra, the extinction coefficients depend on the factor $\Gamma(\alpha - 1)/\Gamma(\alpha - 3/2)$, where α is the parameter of the spectra. As mentioned above, for the Kolmogorov turbulence, $\alpha = 11/6$. Therefore, the ratio of the extinction coefficients for non-Kolmogorov turbulence to those for the Kolmogorov case is given by

$$\gamma_\alpha/\gamma_K = \frac{\Gamma(1/3)\Gamma(\alpha - 1)}{\Gamma(5/6)\Gamma(\alpha - 3/2)}. \tag{37}$$

Here, γ_α is one of the extinction coefficients considered so far (e.g., $\gamma(z)$ or $\bar{\gamma}(h)$) and γ_K is its value for $\alpha = 11/6$. The ratio γ_α/γ_K increases with increasing α and is equal to 1.18 for intermittent turbulence with $\alpha = 23/12$.

3.3. Numerical results

In the numerical results below, we assume that the sound frequency is $f = 1$ kHz, the boundary layer height is $z_i = 700$ m, and the temperature is $T_r = 291$ K at the height $z_r = 1$ m. We also consider the ordinary von Kármán spectra, for which $\alpha = 11/6$.

3.3.1. Horizontal propagation

First, we consider the extinction coefficient γ for horizontal sound propagation.

Figure 3 depicts the extinction coefficient versus the surface heat flux Q_H for three values of the friction velocity u_*. The limiting values $Q_H = 0\,\text{W/m}^2$ and $400\,\text{W/m}^2$ are characteristic of cloudy and sunny conditions, respectively; the values $u_* = 0.05$ m/s, 0.3 m/s, and 0.7 m/s represent light, moderate, and strong wind. In Figure 3, the left plot corresponds to the height $z = 2$ m above the ground, while the right plot to $z = 100$ m. It follows from the figure that the extinction coefficient varies in a wide range, from $10^{-4}\,\text{m}^{-1}$ to about $1\,\text{m}^{-1}$, and increases with increasing heat flux. For $z = 100$ m, the extinction coefficient also increases with increasing friction velocity, while for

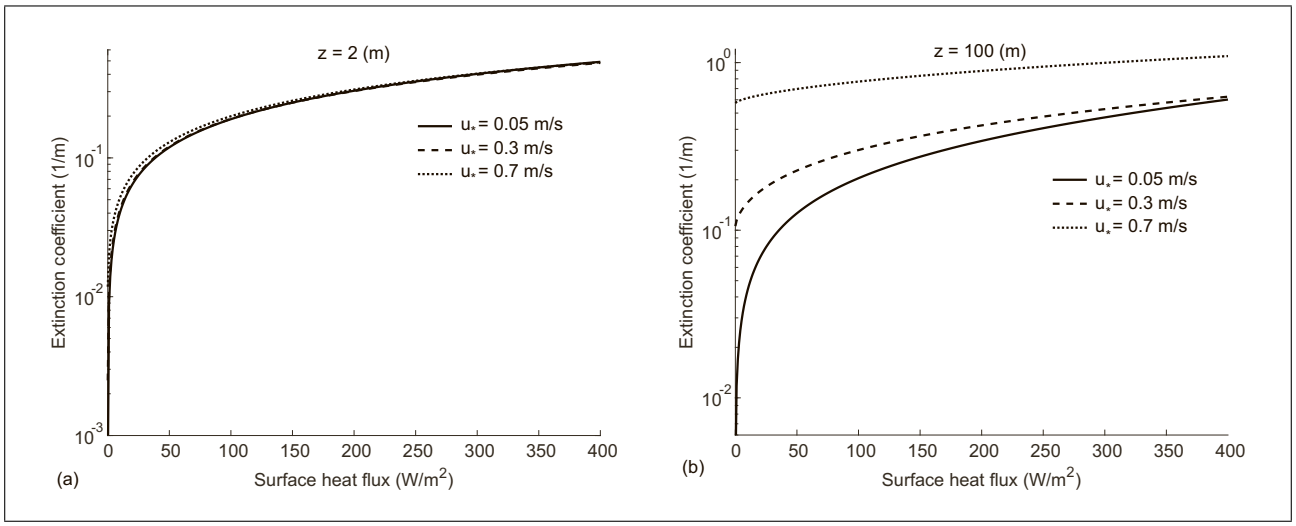

Figure 3. Extinction coefficient γ for horizontal propagation versus the surface heat flux Q_H for three values of the friction velocity u_*. The sound frequency is $f = 1$ kHz. The height above the ground is (left) $z = 2$ m and (right) $z = 100$ m.

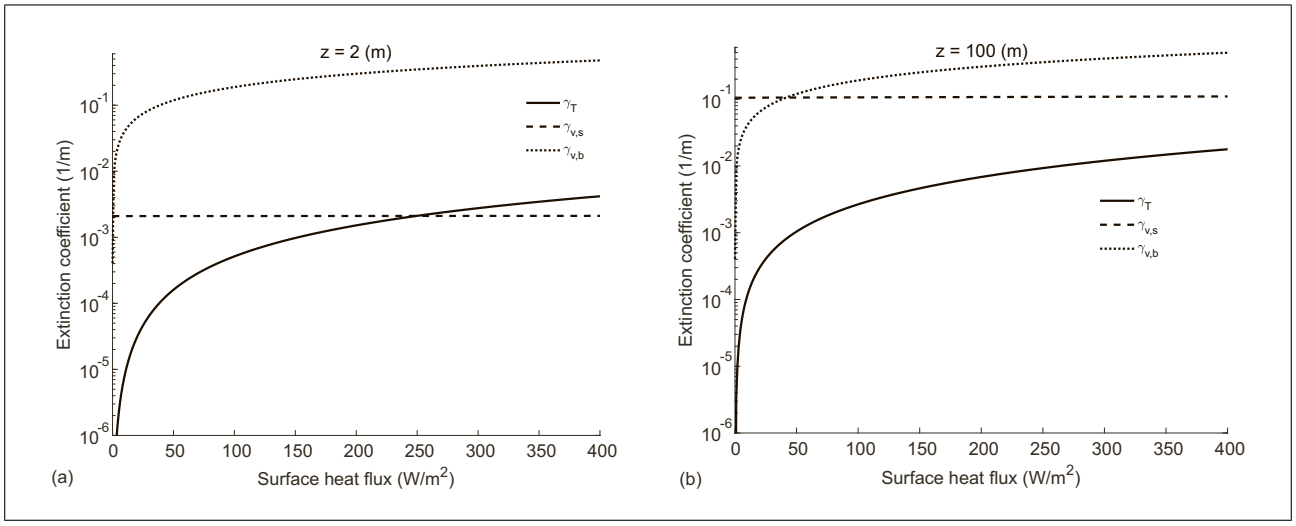

Figure 4. Three contributions, γ_T, $\gamma_{v,s}$, and $\gamma_{v,b}$, to the extinction coefficient γ plotted in Figure 3 for the friction velocity $u_* = 0.3$ m/s.

$z = 2$ m, there is practically no dependence on the friction velocity.

The reason for the different dependence on u_* in Figure 3 can be understood by considering the three contributions to the extinction coefficient, γ_T, $\gamma_{v,s}$, and $\gamma_{v,b}$. These contributions are plotted in Figure 4 versus Q_H for $u_* = 0.3$ m/s. It follows from the figure that γ_T is smaller than $\gamma_{v,b}$ or $\gamma_{v,s}$ and can be ignored. This result is also valid for other friction velocities and heights above the ground. It also follows from Figure 4 that $\gamma_{v,b} \gg \gamma_{v,s}$ for $z = 2$ m. Since $\gamma_{v,b}$ does not depend on the friction velocity, there is little dependence of $\bar{\gamma}$ on u_* at $z = 2$ m (Figure 3). For $z = 100$ m, $\gamma_{v,b}$ can be smaller or large than $\gamma_{v,s}$ depending on the values of Q_H (Figure 4). Since $\gamma_{v,s}$ depends on u_* so does γ in the right plot in Figure 3.

Although not shown here for brevity, the results similar to Figure 4 were also obtained for the friction velocities 0.05 m/s and 0.7 m/s. According to these results, $\gamma_{v,b} \gg \gamma_{v,s}$ for $z = 2$ m. For $z = 100$ m, this inequality still holds if $u_* = 0.05$ m/s, while for $u_* = 0.7$ m/s, we have $\gamma_{v,b} < \gamma_{v,s}$.

3.3.2. Vertical propagation

Figure 5 depicts the extinction coefficient $\bar{\gamma}$ versus the surface heat flux Q_H for three values of the friction velocity u_*. For the left plot, the receiver height is $h = 100$ m, and for the right plot, $h = 200$ m. The extinction coefficient varies from 6×10^{-3} m^{-1} to about 1 m^{-1}. The extinction coefficient $\bar{\gamma}(h = 200\,\text{m})$ is dramatically different from $\gamma(z = 2\,\text{m})$, but is almost identical to $\gamma(z = 100\,\text{m})$ (Figure 3). The reason for the latter result is the following: the temperature contributions to the extinction coefficients $\bar{\gamma}$ and γ are negligible; $\bar{\gamma}_{v,b} = \gamma_{v,b}$ does not depend on height; and $\bar{\gamma}_{v,s}$ and $\gamma_{v,s}$ are related by Equation (35). As a result, the extinction coefficient $\bar{\gamma}(h)$ for vertical propagation is approximately equal to the extinction coefficient $\gamma(z = h/2)$ for horizontal propagation calculated at the receiver half height. For the receiver at $h = 100$ m, the dependence of $\bar{\gamma}$ on Q_H and u_* is about the same as for $h = 200$ m, but the values of $\bar{\gamma}$ are smaller.

Figure 6 depicts three contributions, $\bar{\gamma}_T$, $\bar{\gamma}_{v,s}$, and $\bar{\gamma}_{v,b}$, to the extinction coefficient plotted in Figure 5, for the

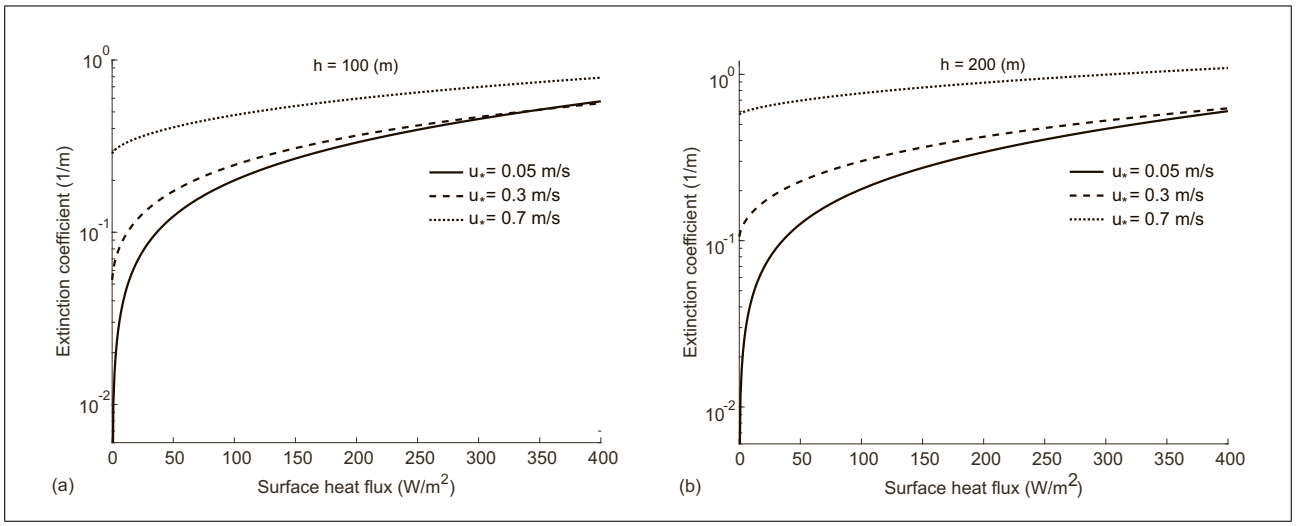

Figure 5. Extinction coefficient $\bar{\gamma}$ for vertical propagation versus the surface heat flux Q_H for three values of the friction velocity u_*. The sound frequency is $f = 1$ kHz. A source is on the ground and the receiver height is (left) $h = 100$ m and (right) $h = 200$ m.

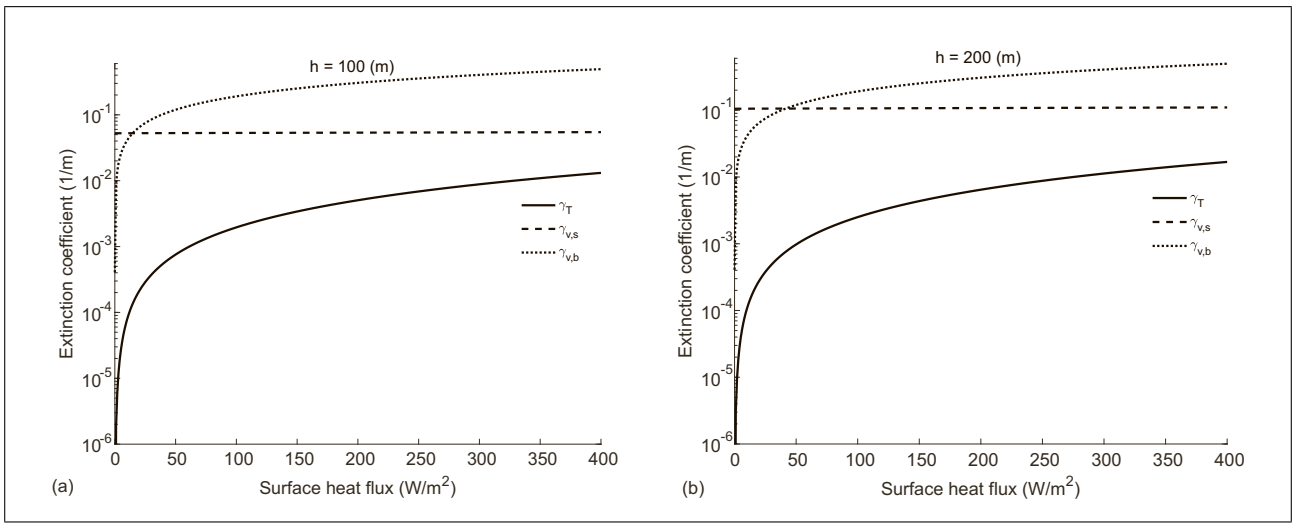

Figure 6. Three contributions, $\bar{\gamma}_T$, $\bar{\gamma}_{v,s}$, and $\bar{\gamma}_{v,b}$, to the extinction coefficient $\bar{\gamma}$ plotted in Figure 5 for the friction velocity $u_* = 0.3$ m/s.

friction velocity $u_* = 0.3$ m/s. The extinction coefficients $\bar{\gamma}_{v,s}$, and $\bar{\gamma}_{v,b}$ are comparable for most values of the surface heat flux. Similarly to horizontal propagation, the extinction coefficient $\bar{\gamma}_T$ is smaller than $\bar{\gamma}_{v,s}$ and $\bar{\gamma}_{v,b}$ so that the temperature contributions to $\bar{\gamma}$ are insignificant.

4. Strength parameter for slanted propagation

In the literature on wave propagation in random media, the strength parameter Φ^2 is defined as the variance of the phase fluctuations in the geometrical acoustics approximation, $\langle \phi^2 \rangle$. The strength parameter enables simplification of formulations for the statistical moments of the sound field.

For horizontal sound propagation in a turbulent atmosphere, the strength parameter $\Phi^2(x; z)$ can be expressed as a sum of the strength parameters due to temperature and wind velocity fluctuations, $\Phi_T^2(x; z)$ and $\Phi_v^2(x; z)$. The strength parameters and the extinction coefficients are related by [18]

$$\Phi^2(x; z) = 2x\gamma(z) = \Phi_T^2(x; z) + \Phi_v^2(x; z) = 2x\gamma_T(z) + 2x\gamma_v(z). \quad (38)$$

For slanted propagation from the ground-based source to the elevated receiver (Figure 1), the strength parameter $\bar{\Phi}_{sl}^2(L; h)$ can also be defined as the variance of the phase fluctuations in the geometrical acoustics approximation. For isotropic turbulence, using Equation (7.79) in [2] and taking into account that Φ_{eff} depends on the height $z = l\cos\theta$ of the point on the propagation path, we have

$$\bar{\Phi}_{sl}^2(L; h) = \left\langle \phi^2 \right\rangle = \pi^2 k^2 \int_0^L \mathrm{d}l \int_0^\infty \Phi_{\text{eff}}(l\cos\theta; \kappa)\kappa\,\mathrm{d}\kappa. \quad (39)$$

Here, similarly to Equation (25), l is the integration variable from the source to the receiver.

Comparing Equations (39) and (25), we obtain

$$\bar{\Phi}^2_{sl}(L;h) = 2L\bar{\gamma}(h). \tag{40}$$

Let $\bar{\Phi}^2$ be the strength parameter for vertical propagation. Setting $L = h$ in Equation (40), we have

$$\bar{\Phi}^2(h) = 2h\bar{\gamma}(h). \tag{41}$$

Comparing this equation with Equation (40) and taking into account that $L = h/\cos\theta$, we obtain a relationship between the strength parameters for slanted and vertical paths,

$$\bar{\Phi}^2_{sl}(L;h) = \frac{\bar{\Phi}^2(h)}{\cos\theta}. \tag{42}$$

Thus, the strength parameter for slanted propagation from the ground-based source to the elevated receiver is expressed in terms of that for vertical propagation and the propagation angle θ. For vertical propagation, the strength parameter and the extinction coefficient are related by a simple formula (Equation (41)), which makes them interchangeable in equations for the statistical moments of the sound field. Similarly to Section 3.2 it can be shown that if the turbulence parameters do not depend on the height above the ground or if the propagation angle $\theta \to 0$, the strength parameter $\bar{\Phi}^2_{sl}$ coincides with that for horizontal propagation. Furthermore, Equations (40)-(42) are also valid for the elevated source and ground-based receiver.

Let $\bar{\Phi}^2_T(h)$ and $\bar{\Phi}^2_v(h)$ be the strength parameters due to temperature and velocity fluctuations for a vertical path. Then,

$$\bar{\Phi}^2(h) = \bar{\Phi}^2_T(h) + \bar{\Phi}^2_v(h), \tag{43}$$

$$\bar{\Phi}^2_T(h) = 2h\bar{\gamma}_T(h), \quad \bar{\Phi}^2_v(h) = 2h\bar{\gamma}_v(h). \tag{44}$$

5. Mutual coherence function

The transverse mutual coherence function (MCF) is an important statistical characteristics of the sound field. It is used in applications for determining a maximum separation between microphones at which the coherent signal processing is feasible. In this section, the MCF is studied for slanted propagation.

5.1. Normalized spectra of turbulence

The MCF can be expressed in a compact form useful for further analysis by employing normalized non-dimensional spectra of temperature and velocity fluctuations, $\hat{\Phi}_T$ and $\hat{\Phi}_v$. For horizontal propagation, such spectra were introduced in [18].

The normalized non-dimensional spectra are defined as [18, 19]

$$\hat{\Phi}_T(z,\hat{\kappa}) = \frac{2\pi^2}{\sigma^2_T(z)\mathcal{L}_T(z)L^2_T(z)}\tilde{\Phi}_T(z,\hat{\kappa}), \tag{45}$$

$$\hat{\Phi}_v(z,\hat{\kappa}) = \frac{\pi}{2\sigma^2_v(z)\mathcal{L}_v(z)}\frac{E(z,\hat{\kappa})}{\hat{\kappa}^2}. \tag{46}$$

In Equation (45), $\hat{\kappa} = \kappa L_T$, and in Equation (46), $\hat{\kappa} = \kappa L_v$, where $L_T(z)$ and $L_v(z)$ are the characteristic length scales of the spectra. For the generalized von Kármán spectra, these length scales are chosen as those appearing in Equations (1) and (2); for other spectra, $L_T(z)$ and $L_v(z)$ can be chosen as suggested in [18]. The spectra $\hat{\Phi}_T(z,\hat{\kappa})$ and $\hat{\Phi}_v(z,\hat{\kappa})$ satisfy the following normalization condition,

$$\int_0^\infty \hat{\Phi}_{T,v}(z,\hat{\kappa})\,\hat{\kappa}\,\mathrm{d}\hat{\kappa} = 1. \tag{47}$$

Here the subscript T, v implies that a quantity such as $\hat{\Phi}_{T,v}$ can be either $\hat{\Phi}_T$ or $\hat{\Phi}_v$. The equality (47) can be verified by substituting with Equations (45) and (46) and accounting for the definitions of the integral length scales $\mathcal{L}_T$ and $\mathcal{L}_v$, Equations (3) and (4).

It follows from Equations (15) and (16) that

$\sigma^2_T(z)\mathcal{L}_T(z) = 4T^2_0\gamma_T(z)/k^2$

and

$\sigma^2_v(z)\mathcal{L}_v(z) = c^2_0\gamma_v(z)/k^2$.

Using these relationships in Equations (45) and (46) and solving for $\tilde{\Phi}_T$ and E, we have

$$\tilde{\Phi}_T(z,\hat{\kappa}) = \frac{2T^2_0\gamma_T(z)L^2_T(z)}{\pi^2k^2}\hat{\Phi}_T(z,\hat{\kappa}), \tag{48}$$

$$E(z,\hat{\kappa}) = \frac{2c^2_0\gamma_v(z)\hat{\kappa}^2}{\pi k^2}\hat{\Phi}_v(z,\hat{\kappa}). \tag{49}$$

These formulas express the spectra of temperature and velocity fluctuations in terms of the corresponding extinction coefficients and normalized spectra. The results above are valid for arbitrary spectra of turbulence.

For the generalized von Kármán spectra, the normalized non-dimensional spectra are obtained by substituting with Equations (1) and (2) and accounting for Equations (5) and (6),

$$\hat{\Phi}_T(\hat{\kappa}) = \frac{2(\alpha-1)}{\left(1+\hat{\kappa}^2\right)^\alpha}, \quad \hat{\Phi}_v(\hat{\kappa}) = \frac{2(\alpha-1)\alpha\hat{\kappa}^2}{\left(1+\hat{\kappa}^2\right)^{\alpha+1}}. \tag{50}$$

These spectra do not depend on the height above the ground.

5.2. MCF for arbitrary spectra of turbulence

The transverse MCF of the sound field is defined as

$$\Gamma(L,\mathbf{r}) = \left\langle p(L,\mathbf{r}/2)\,p^*(L,-\mathbf{r}/2)\right\rangle. \tag{51}$$

Here, L is the length of the propagation path and $\mathbf{r}$ is the vector between two observation points, $\mathbf{r}$ being perpendicular to the propagation path.

For horizontal sound propagation at the height z above the ground, the MCF due to a point source is given by Equation (7.183) in [2],

$$\Gamma(x,r) = |p_0|^2 \exp\left\{-\pi^2k^2\int_0^x \mathrm{d}x' \cdot \int_0^\infty \Phi_{\mathrm{eff}}(z;\kappa)\left[1-J_0\left(x'\kappa r/x\right)\right]\kappa\,\mathrm{d}\kappa\right\}, \tag{52}$$

where x is the horizontal propagation range and J_0 is the Bessel function.

Consider slanted sound propagation from a ground-based source to an elevated receiver. For this geometry, the MCF of a point source is given by Equation (7.181) in [2]. For isotropic turbulence, this equation simplifies to

$$\Gamma(L,r) = |p_0|^2 \exp\left\{ -\pi^2 k^2 \int_0^L \mathrm{d}l \cdot \int_0^\infty \Phi_{\mathrm{eff}}(l\cos\theta;\kappa)\left[1 - J_0(l\kappa r/L)\right]\kappa\,\mathrm{d}\kappa \right\}, \tag{53}$$

where, similarly to Equation (25), l is the integration variable along the propagation path (Figure 1). In Equation (53), the expression in the exponential is equal to $(1/2)D_\phi(L,r)$, where D_ϕ is the structure function of the phase fluctuations calculated in geometrical acoustics. Transforming from the integration variable l to the height above the ground $z = l\cos\theta$, we obtain

$$D_\phi = \frac{2\pi^2 k^2}{\cos\theta}\int_0^h \mathrm{d}z \cdot \int_0^\infty \Phi_{\mathrm{eff}}(z;\kappa)\left[1 - J_0(z\kappa r/h)\right]\kappa\,\mathrm{d}\kappa. \tag{54}$$

The right-hand side of this equation can be split into two integrals corresponding to the two terms in the square bracket. Accounting for Equation (26), the first integral is equal to $2h\bar{\gamma}/\cos\theta = 2h(\bar{\gamma}_T + \bar{\gamma}_v)/\cos\theta$. In the second integral, $\Phi_{\mathrm{eff}}(z;\kappa)$ is given by Equation (13). With these manipulations, the structure function becomes

$$D_\phi = \frac{2}{\cos\theta}\left\{ 2h\bar{\gamma}_T(h) + 2h\bar{\gamma}_v(h) - \int_0^h \mathrm{d}z \int_0^\infty \mathrm{d}\kappa \cdot \left[\frac{\pi^2 k^2}{T_0^2}\tilde{\Phi}_T(z;\kappa)\kappa + \frac{\pi k^2}{c_0^2}\frac{E(z;\kappa)}{\kappa}\right] J_0(z\kappa r/h) \right\}. \tag{55}$$

Using Equations (48) and (49), the spectra $\tilde{\Phi}_T(z;\kappa)$ and $E(z;\kappa)$ are expressed in terms of the normalized spectra of temperature and velocity fluctuations. Rearanging terms in the exponential, we have

$$D_\phi(L,r) = \frac{2}{\cos\theta}\left\{ 2h\bar{\gamma}_T(h) - 2\int_0^h \mathrm{d}z\,\gamma_T(z) \cdot \int_0^\infty \hat{\Phi}_T(z;\hat{\kappa})\,J_0\left(\frac{z\hat{\kappa}r}{hL_T(z)}\right)\hat{\kappa}\,\mathrm{d}\kappa + 2h\bar{\gamma}_v(h) - 2\int_0^h \mathrm{d}z\,\gamma_v(z)\int_0^\infty \hat{\Phi}_v(z;\hat{\kappa})\,J_0\left(\frac{z\hat{\kappa}r}{hL_v(z)}\right)\hat{\kappa}\,\mathrm{d}\kappa \right\}. \tag{56}$$

Here, we introduce a new integration variable $\eta = z/h$, factor out $2h\bar{\gamma}_T(h)$ from the the first two terms, and $2h\bar{\gamma}_v(h)$ from the third and fourth terms. Substituting the result into Equation (53), we obtain

$$\Gamma(L,r) = |p_0|^2 \exp\left\{ -\frac{\bar{\Phi}_T^2(h)}{\cos\theta}\left[1 - \Psi_T(h,r)\right] - \frac{\bar{\Phi}_v^2(h)}{\cos\theta}\left[1 - \Psi_v(h,r)\right] \right\}. \tag{57}$$

In this formula, the strength parameters $\bar{\Phi}_{T,v}^2$ are determined with Equation (44) and the non-dimensional functions $\Psi_{T,v}$ are given by

$$\Psi_{T,v}(h,r) = \int_0^1 \mathrm{d}\eta\,\mu_{T,v}(\eta,h) \cdot \int_0^\infty \hat{\Phi}_{T,v}(\eta h;\hat{\kappa})\,J_0\left(\frac{\eta\hat{\kappa}r}{L_{T,v}(\eta h)}\right)\hat{\kappa}\,\mathrm{d}\hat{\kappa}, \tag{58}$$

where

$$\mu_{T,v}(\eta,h) = \frac{\gamma_{T,v}(\eta h)}{\bar{\gamma}_{T,v}(h)}. \tag{59}$$

The functions $\Psi_{T,v}(h,r)$ characterize the dependence of the MCF on the sensor separation r. They can be evaluated for small and large values of r. For $r \ll L_{T,v}$, the Bessel function J_0 can be set to unity. In this case, the integral over $\hat{\kappa}$ is unity due to the normalization condition, Equation (47). The remaining integral over η is also unity,

$$\int_0^1 \mu_{T,v}(\eta,h)\,\mathrm{d}\eta = 1. \tag{60}$$

This equality can be verified by substituting with Equation (59), factoring out $\bar{\gamma}_{T,v}(h)$ from the integral, and accounting for Equation (30). For $r \gg L_{T,v}$, the Bessel function J_0 in Equation (58) oscillates rapidly so that $\Psi_{T,v}(h,r) \approx 0$. Thus, for small and large values of r, the non-dimensional functions $\Psi_{T,v}(h,r)$ are

$$r/L_{T,v} \ll 1: \quad \Psi_{T,v}(h,r) \approx 1; \tag{61}$$

$$r/L_{T,v} \gg 1: \quad \Psi_{T,v}(h,r) \approx 0. \tag{62}$$

For plausible spectra of turbulence, we expect that the functions $\Psi_{T,v}(h,r)$ decrease smoothly from unity to zero with increasing sensor separation.

Equation (57) for the MCF for slanted propagation is a new result of this paper. This equation is valid for arbitrary spectra of temperature and velocity fluctuations. Similarly to the extinction coefficient, the MCF for a slanted path differs from that for a vertical path only by the factor $1/\cos\theta$ in the exponential. A compact form of Equation (57) enables a general analysis of $\Gamma(L,r)$. First, in Equation (58), $J_0(\eta\hat{\kappa}r/L_{T,v}(\eta h))$ is a "weighting" function along the propagation path. Due to this function, the turbulence near the source ($\eta \sim 0$) practically does not affect $\Gamma(L,r)$, while the turbulence near the receiver ($\eta \sim 1$), generally, has the most effect. Second, using the limiting values of the functions $\Psi_{T,v}(h,r)$ given by Equations (61) and (62), the MCF can be evaluated for small and large values of the sensor separation,

$$r/L_{T,v} \ll 1: \quad \Gamma(L,r) \approx |p_0|^2; \tag{63}$$

$$r/L_{T,v} \gg 1: \quad \Gamma(L,r) \approx |p_0|^2 \exp\left[-\frac{\bar{\Phi}_T^2(h)}{\cos\theta} - \frac{\bar{\Phi}_v^2(h)}{\cos\theta}\right]. \tag{64}$$

If the variances and length scales of turbulence do not depend on z or if $\theta \to 0$, the functions $\Psi_{T,v}$ and the MCF $\Gamma(L,r)$ coincide with similar functions for horizontal propagation given by Equations (70) and (72) in [18].

5.3. Generalized von Kármán spectra

Here, the results from the previous subsection are specified for the generalized von Kármán spectra.

Substituting Equation (50) into Equation (58) and calculating the integrals over $\hat{\kappa}$ similarly to that in [18], we have

$$\Psi_T(h,r) = \frac{2^{2-\alpha}}{\Gamma(\alpha-1)} \int_0^1 \mu_T(\eta h, h) \left(\frac{\eta r}{L_T(\eta h)}\right)^{\alpha-1} \cdot K_{\alpha-1}\left(\frac{\eta r}{L_T(\eta h)}\right) \mathrm{d}\eta, \tag{65}$$

$$\Psi_v(h,r) = \frac{2^{2-\alpha}}{\Gamma(\alpha-1)} \int_0^1 \mu_v(\eta h, h) \left(\frac{\eta r}{L_v(\eta h)}\right)^{\alpha-1} \cdot \left[K_{\alpha-1}\left(\frac{\eta r}{L_v(\eta h)}\right) - \frac{\eta r}{2L_v(\eta h)} K_{2-\alpha}\left(\frac{\eta r}{L_v(\eta h)}\right)\right] \mathrm{d}\eta. \tag{66}$$

Here K_α is the modified Bessel function of the second kind. For $\mu_{T,v} = 1$ and $L_{T,v} =$ constant, these formulas coincide with Equations (77) and (78) in [18].

Taking into account that the wind velocity fluctuations are due to shear and buoyancy, the MCF can be written as

$$\Gamma(L,r) = |p_0|^2 \exp\left\{-\frac{\bar{\Phi}_T^2(h)}{\cos\theta}\left[1-\Psi_T(h,r)\right] - \frac{\bar{\Phi}_{v,s}^2(h)}{\cos\theta}\left[1-\Psi_{v,s}(h,r)\right] - \frac{\bar{\Phi}_{v,b}^2(h)}{\cos\theta}\left[1-\Psi_{v,b}(h,r)\right]\right\}. \tag{67}$$

In this formula, the functions $\Psi_{v,s}$ and $\Psi_{v,b}$ are given by Equation (66), where L_v equals $L_{v,s}$ and $L_{v,b}$, respectively. Equation (67) can also be written as

$$\Gamma(L,r) = |p_0|^2 \Gamma_T(L,r) \Gamma_{v,s}(L,r) \Gamma_{v,b}(L,r). \tag{68}$$

Here, Γ_T, $\Gamma_{v,s}$, and $\Gamma_{v,b}$ are the contributions to the MCF due to temperature and velocity fluctuations, given by

$$\Gamma_\tau(L,r) = \exp\left[-\frac{\bar{\Phi}_\tau^2(h)}{\cos\theta}\left[1-\Psi_\tau(h,r)\right]\right], \tag{69}$$

where the subscript τ stands for T, v,b, or v,s. These three contributions to the MCF are similar to those for the extinction coefficient and enable us to determine what type of fluctuations in the turbulent atmosphere result in the coherence loss.

Some quantities appearing in Equation (67) can be specified further. The strength parameters can be expressed in terms of the extinction coefficients $\bar{\gamma}_T(h)$, $\bar{\gamma}_{v,s}(h)$, and $\bar{\gamma}_{v,b}(h)$, which were calculated in Section 3. Using results from that section and Equation (59), we can also calculate the functions $\mu_{T,v}(\eta h, h)$ in Equations (65) and (66). For the temperature contribution, we have

$$\mu_T(\eta h, h) = \frac{F_{\mathrm{hor}}\left(\frac{10\eta h}{-L_o}\right)}{F_{\mathrm{ver}}\left(\frac{10h}{-L_o}\right)}. \tag{70}$$

For the velocity contributions,

$$\mu_{v,s}(\eta h, h) = 2\eta, \quad \mu_{v,b}(\eta h, h) = 1. \tag{71}$$

In Equations (65) and (66), the arguments of the modified Bessel functions K_α are denoted as $\varrho_{T,v} = \eta r / L_{T,v}(\eta h)$. The functions $\varrho_{T,v}$ also appear in the integrands of these equations. For temperature fluctuations, we have

$$\varrho_T = \frac{r}{2h} \frac{1 - 10\eta h/L_o}{1 - 7\eta h/L_o}, \tag{72}$$

and for velocity fluctuations,

$$\varrho_{v,s} = \frac{r}{1.8h}, \quad \varrho_{v,b} = \frac{\eta r}{L_{v,b}}. \tag{73}$$

Since $\varrho_{v,s}$ does not depend on the integration variable η, the corresponding integral can be evaluated analytically,

$$\Psi_{v,s}(h,r) = \frac{2^{2-\alpha}}{\Gamma(\alpha-1)} \varrho_{v,s}^{\alpha-1} \cdot \left[K_{\alpha-1}(\varrho_{v,s}) - \frac{\varrho_{v,s}}{2} K_{2-\alpha}(\varrho_{v,s})\right]. \tag{74}$$

5.4. Elevated source

For an elevated source and ground-based receiver, the coherence function is given by Equation (53), if the integration is performed from the elevated source ($l = 0$) to the ground-based receiver ($l = L$) and $\Phi_{\mathrm{eff}} = \Phi_{\mathrm{eff}}((L-l)\cos\theta); \kappa)$, where $z = (L-l)\cos\theta$ is the height above the ground. Using the same manipulations as in Section 5.2, it can be shown that the MCF is still given by Equation (57), where the non-dimensional functions $\Psi_{T,v}$ are

$$\Psi_{T,v}(h,r) = \int_0^1 \mathrm{d}\eta\, \mu_{T,v}(\eta, h) \cdot \int_0^\infty \hat{\Phi}_{T,v}(\eta h; \hat{\kappa})\, J_0\left(\frac{(1-\eta)\hat{\kappa} r}{L_{T,v}(\eta h)}\right) \hat{\kappa}\, \mathrm{d}\hat{\kappa}. \tag{75}$$

The difference between this formula and Equation (58) is that the integration variable η in the argument of the Bessel function J_0 is replaced with $1-\eta$. As a result, the weighting functions in Equations (58) and (75) are different so that there is no reciprocity for the MCF due to a point source. For the elevated source, the strength parameters $\bar{\Phi}_{T,v}^2(h)$ and the functions $\mu_{T,v}(\eta h, h)$ remain the same as those for the ground-based source.

For the generalized von Kármán spectra, it can be shown that $\Psi_{T,v}$ are given by Equations (65) and (66) if the functions $\varrho_{T,v} = \eta r / L_{T,v}(\eta h)$ in the integrands and arguments of K_α are replaced with $\varrho_{T,v} = (1-\eta) r / L_{T,v}(\eta h)$.

5.5. Numerical results

Figure 7 depicts the MCF $\Gamma(L,r)$ for vertical sound propagation from the ground-based source to the elevated receiver, normalized by $|p_0|^2$, versus the sensor separation r, for three values of the surface heat flux Q_H. The friction velocity is $u_* = 0.3$ m/s and the receiver height is (left plot) $h = 200$ m and (right plot) $h = 400$ m.

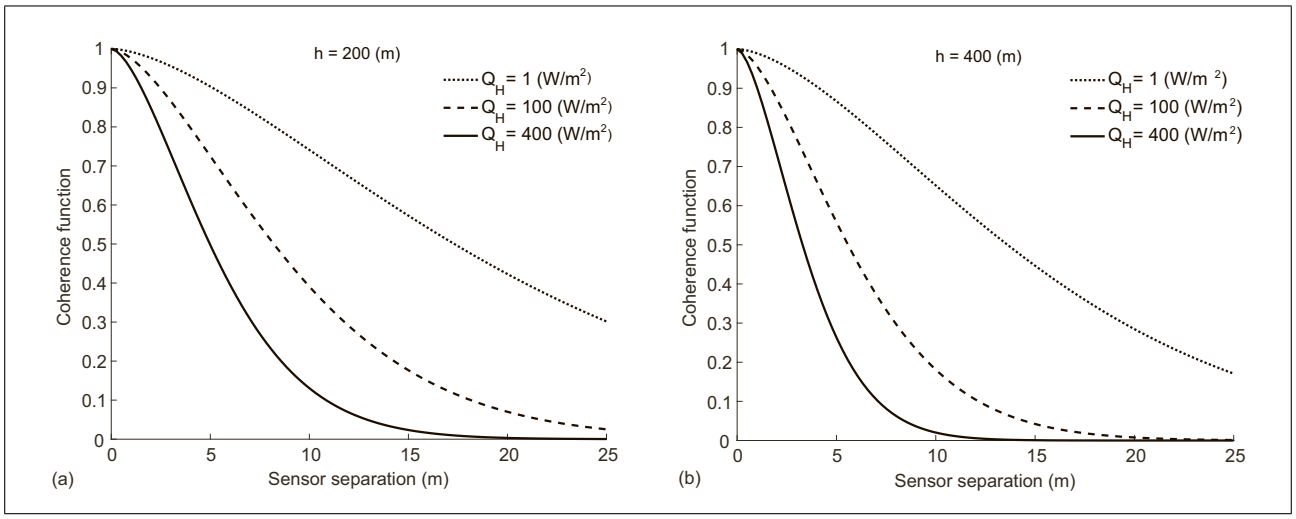

Figure 7. Mutual coherence function, normalized by $|p_0|^2$, versus sensor separation r for vertical propagation and three values of the surface heat flux Q_H. The sound frequency is $f = 1$ kHz. The receiver height is (left) $h = 200$ m and (right) $h = 400$ m.

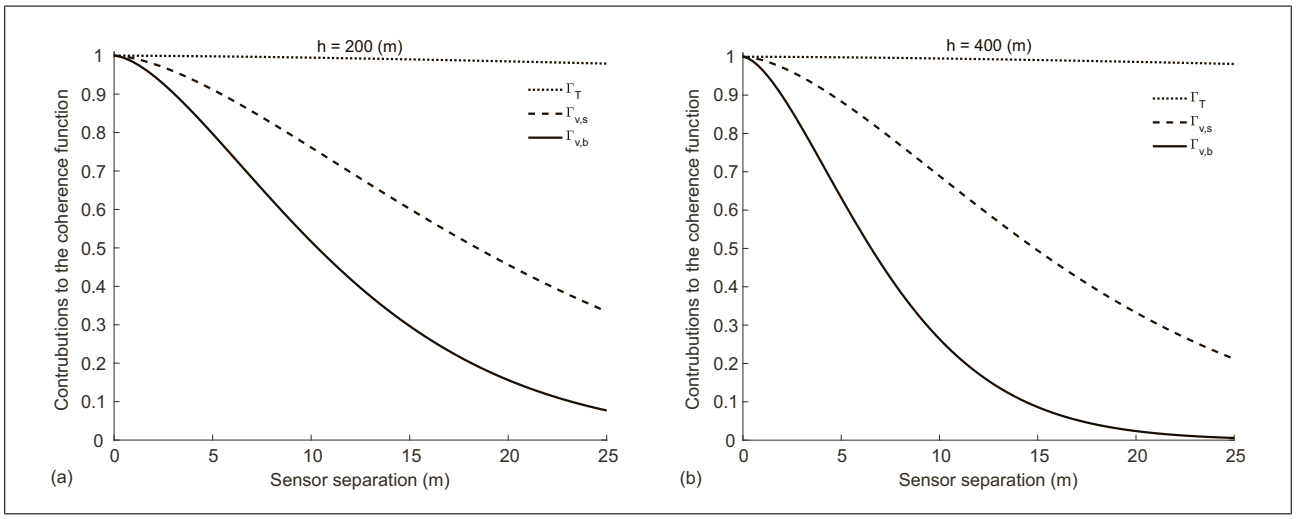

Figure 8. Three contributions, Γ_T, $\Gamma_{v,s}$, and $\Gamma_{v,b}$, to the mutual coherence function (MCF) plotted in Figure 7 for the surface heat flux $Q_H = 100$ W/m^2.

It follows from Figure 7 that $\Gamma(L, r)$ monotonically decreases with increasing sensor separation as it should. The coherence radius r_c is an important parameter of the MCF, defined as

$$\Gamma(L, r_c) = \exp(-1)\Gamma(L, r = 0). \tag{76}$$

According to this equation, the coherence radius is equal to the microphone separation at which the coherence decreases by a factor $\exp(-1) \approx 0.368$. Using this definition, the coherence radii of the mutual coherence functions in Figure 7 can be determined. For $h = 200$ m (Figure 7, left plot), the coherence radius decreases with increasing surface heat flux and is equal $r_c = 22.1$ m, 10.4 m, and 6.3 m, respectively. For a longer vertical path $h = 400$ m (Figure 7, right plot), the coherence radius is smaller: $r_c = 17.2$ m, 7.1 m, and 4.2 m.

Consider the MCF for $Q_H = 100$ W/m^2 (Figure 7). The temperature and velocity contributions to this function, Γ_T, $\Gamma_{v,s}$, and $\Gamma_{v,b}$, are depicted in Figure 8. It follows from the figure that for both $h = 200$ m and 400 m, the two velocity contributions are comparable. The temperature contribution is close to unity and, therefore, does not significantly affect the MCF.

Solid lines in the left plot in Figure 9 depict the coherence radius r_c for vertical propagation versus the surface heat flux Q_H for three values of the friction velocity u_*. The height of the receiver is $h = 200$ m. The coherence radius ranges from about 5 m to more than 50 m and decreases with increasing Q_H and u_*. Dashed lines in the left plot correspond to the coherence radius for horizontal sound propagation at the height $z = 2$ m calculated with Equation (52). The horizontal propagation range $x = 200$ m is the same as the vertical range $h = 200$ m. The coherence radius for horizontal propagation has a similar dependence on Q_H and u_* as that for vertical propagation, but it is significantly smaller, especially for large values of Q_H and u_*. The ratio between the two coherence radii can be as large as 3.18.

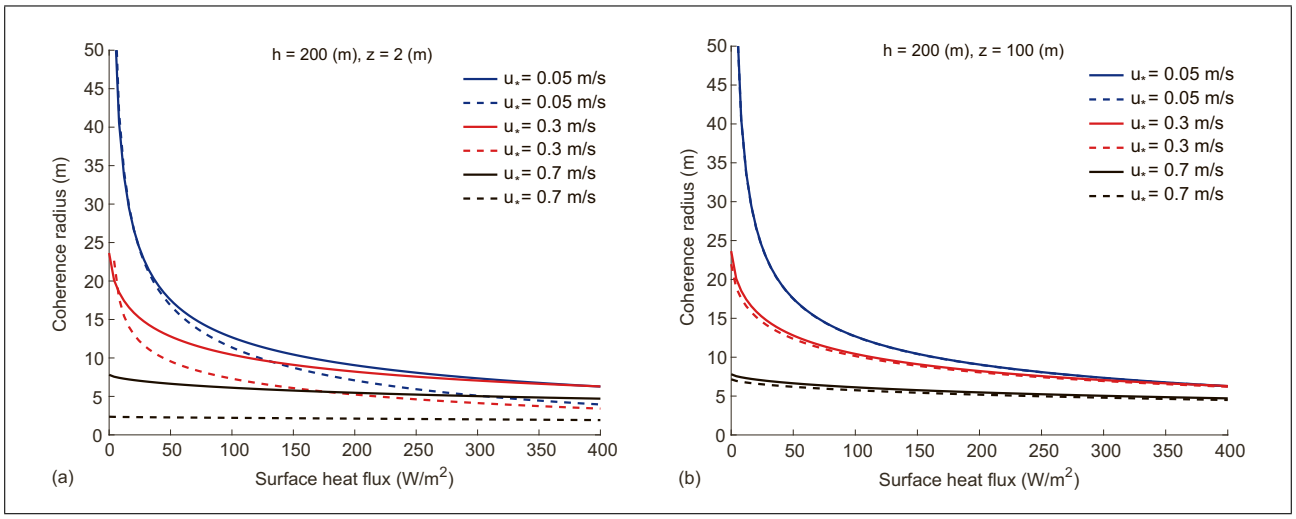

Figure 9. The coherence radius r_c versus the surface heat flux Q_H for three values of the friction velocity u_*. The sound frequency is $f = 1$ kHz. Solid lines correspond to vertical propagation and the receiver height $h = 200$ m. Dashed lines correspond to horizontal propagation at the height above the ground (left) $z = 2$ m and (right) $z = 100$ m.

The solid lines in the left plot in Figure 9 are reproduced in the right plot. The dashed lines correspond to the coherence radius for horizontal sound propagation at the height $z = 100$ m; the range is the same, $x = 200$ m. It follows from the figure that the coherence radii for vertical and horizontal propagation at $z = h/2$ are very close. A similar result was obtained for the extinction coefficients of the mean sound field (Section 3.3).

The solid lines in Figure 9 are also reproduced in Figure 10. The dashed lines correspond to the coherence radius for vertical propagation when the source is at the height $h = 200$ m and the receiver is on the ground. The solid lines do not coincide with the dashed lines, which demonstrates the non-reciprocity for the MCF along vertical and slanted paths. The ratio between the two coherence radii can be as large as 1.47.

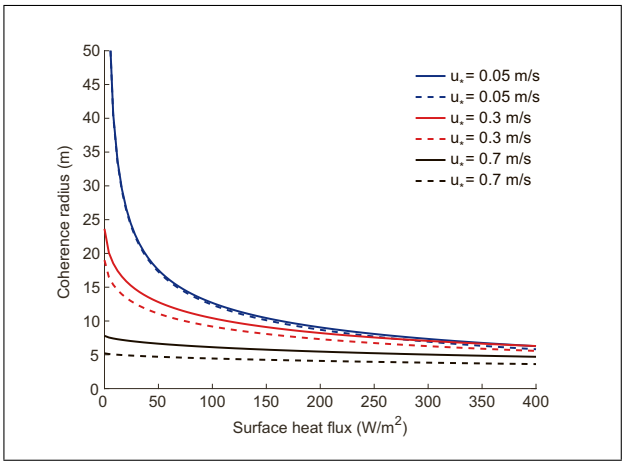

Figure 10. Coherence radius r_c for vertical propagation versus the surface heat flux Q_H for three values of the friction velocity u_*. The sound frequency is $f = 1$ kHz. Solid lines correspond to the ground-based source and the receiver at the height $h = 200$ m. Dashed lines correspond to the source at the height $h = 200$ m and ground-based receiver.

6. Phase and log-amplitude fluctuations

Similarly to the mean sound field and MCF, other statistical characteristics of sound signals propagating over vertical and slanted paths in a turbulent atmosphere can be analyzed. In this section, the results for the correlation functions and variances of the phase and log-amplitude fluctuations are briefly outlined.

6.1. Correlation functions for the ground-based source

First, we consider the case of a ground-based source and elevated receiver (Figure 1). In this case, the correlation functions of the phase and log-amplitude fluctuations, B_ϕ and B_χ, are given by Equations (7.97) and (7.98) in [2]:

$$B_{\phi,\chi}(L,r) = \frac{\pi^2 k^2}{2}\int_0^L \mathrm{d}l \int_0^\infty \Phi_{\mathrm{eff}}(l\cos\theta;\kappa) \cdot J_0\left(l\kappa r/L\right)\left[1 \pm \cos\left(\frac{l}{L}\left(1-\frac{l}{L}\right)\frac{\kappa^2 L}{k}\right)\right]\kappa\,\mathrm{d}\kappa. \tag{77}$$

Here, the upper and lower signs in the square brackets correspond to B_ϕ and B_χ, respectively. Transforming to the integration variable $\eta = l/L = z/h$, we have

$$B_{\phi,\chi}(L,r) = \frac{\pi^2 k^2 h}{2\cos\theta}\int_0^1 \mathrm{d}\eta \int_0^\infty \Phi_{\mathrm{eff}}(\eta h;\kappa) \cdot J_0\left(\eta\kappa r\right)\left[1 \pm \cos\left(\frac{\eta(1-\eta)\kappa^2 L}{k}\right)\right]\kappa\,\mathrm{d}\kappa. \tag{78}$$

Using Equations (13), (48), and (49), the effective spectrum can be expressed in terms of the extinction coefficients for horizontal propagation $\gamma_{T,v}$ and the normalized

non-dimensional spectra $\hat{\Phi}_{T,v}$,

$$\Phi_{\text{eff}}(\eta h;\kappa) = \frac{2\gamma_T(\eta h)\hat{\Phi}_T(\eta h;\hat{\kappa})L_T^2(\eta h)}{\pi^2 k^2} + \frac{2\gamma_v(\eta h)\hat{\Phi}_v(\eta h;\hat{\kappa})L_v^2(\eta h)}{\pi^2 k^2}. \quad (79)$$

Substituting this result into Equation (78) and taking into account Equation (44), we obtain

$$B_{\phi,\chi}(L,r) = \frac{\bar{\Phi}_T^2(h)}{2\cos\theta}\left[\Psi_T(h,r) \pm \tilde{\Psi}_T(L,r)\right] + \frac{\bar{\Phi}_v^2(h)}{2\cos\theta}\left[\Psi_v(h,r) \pm \tilde{\Psi}_v(L,r)\right]. \quad (80)$$

Here, the non-dimensional functions $\Psi_{T,v}(h,r)$ are given by Equation (58) and the new non-dimensional functions $\tilde{\Psi}_{T,v}(L,r)$ are

$$\tilde{\Psi}_{T,v}(L,r) = \int_0^1 \mathrm{d}\eta\, \mu_{T,v}(\eta,h) \int_0^\infty \hat{\Phi}_{T,v}(\eta h;\hat{\kappa}) \cdot J_0\left(\frac{\eta\hat{\kappa}r}{L_{T,v}(\eta h)}\right)\cos\left[\eta(1-\eta)\hat{\kappa}^2 D_{T,v}(L,\eta h)\right]\hat{\kappa}\,\mathrm{d}\hat{\kappa}. \quad (81)$$

The only difference between the functions $\Psi_{T,v}(h,r)$ and $\tilde{\Psi}_{T,v}(L,r)$ is the cosine term in Equation (81). In this term, D_T and D_v are the height-dependent wave parameters for temperature and velocity fluctuations [18],

$$D_{T,v}(L,z) = \frac{L}{kL_{T,v}^2(z)} = \frac{h}{kL_{T,v}^2(z)\cos\theta}. \quad (82)$$

Equation (80) is a new result obtained in the paper. This equation expresses the correlation functions $B_\phi(L,r)$ and $B_\chi(L,r)$ in terms of the strength parameters $\bar{\Phi}_{T,v}^2(h)$ and the non-dimensional functions $\Psi_{T,v}(h,r)$ and $\tilde{\Psi}_{T,v}(L,r)$. Since D_T and D_v depend on the propagation angle θ, the dependence of the correlation functions on this angle is more involved than that for the mean sound field and MCF. Similarly to the extinction coefficient and MCF, the correlation functions for slanted propagation $B_{\phi,\chi}(L,r)$ coincide with those for horizontal propagation if the turbulence parameters do not depend on the height above the ground or if the propagation angle $\theta \to 0$.

The small and large values of the wave parameter $D_{T,v}$ correspond to geometrical acoustics and Fraunhofer diffraction, respectively. For $D_{T,v} \ll 1$, the cosine function in Equation (81) is about unity so that $\tilde{\Psi}_{T,v} \approx \Psi_{T,v}$. For $D_{T,v} \gg 1$, this cosine function oscillates rapidly and $\left|\tilde{\Psi}_{T,v}\right| \ll |\Psi_{T,v}|$. In these limiting cases, the correlation functions simplify,

$$D_{T,v} \ll 1: \quad B_\phi(L,r) = \frac{\bar{\Phi}_T^2(h)}{\cos\theta}\Psi_T(h,r) + \frac{\bar{\Phi}_v^2(h)}{\cos\theta}\Psi_v(h,r), \quad \left|B_\chi(L,r)\right| \ll \left|B_\phi(L,r)\right|; \quad (83)$$

$$D_{T,v} \gg 1: \quad B_\phi(L,r) = B_\chi(L,r) = \frac{\bar{\Phi}_T^2(h)}{2\cos\theta}\Psi_T(h,r) + \frac{\bar{\Phi}_v^2(h)}{2\cos\theta}\Psi_v(h,r). \quad (84)$$

It follows from these formulas that B_ϕ and B_χ are expressed in terms of the strength parameters $\bar{\Phi}_{T,v}^2(h)$ and the non-dimensional functions $\Psi_{T,v}(h,r)$ pertinent to the MCF. The dependence of the correlation functions on the propagation angle is given by the factor $1/\cos\theta$.

For the generalized von Kármán spectra, the correlation functions B_ϕ and B_χ can be analyzed similarly to the approach in Section 5.3. Note that in Equation (80), the strength parameters $\bar{\Phi}_{T,v}^2(h)$ and the non-dimensional functions $\Psi_{T,v}(h,r)$ have already been assessed for these spectra.

6.2. Variances for ground-based sources

The variances of the phase and log-amplitude fluctuations are equal to the correlation functions evaluated at $r = 0$:

$$\left\langle \phi^2 \right\rangle = B_\phi(L,0), \quad \left\langle \chi^2 \right\rangle = B_\chi(L,0). \quad (85)$$

Setting $r = 0$ in Equation (80), we obtain

$$\left\langle \phi^2 \right\rangle, \left\langle \chi^2 \right\rangle = \frac{\bar{\Phi}_T^2(h)}{2\cos\theta}\left[1 \pm \tilde{\Psi}_T(L,0)\right] + \frac{\bar{\Phi}_v^2(h)}{2\cos\theta}\left[1 \pm \tilde{\Psi}_v(L,0)\right]. \quad (86)$$

Here, the upper sign corresponds to $\left\langle \phi^2 \right\rangle$ and the lower sign to $\left\langle \chi^2 \right\rangle$. When deriving this formula, we took into account that according to Equation (61), $\Psi_{T,v}(h,0) = 1$.

In the limiting cases of small and large values of the wave parameter, Equation (86) simplifies to

$$D_{T,v} \ll 1: \quad \left\langle \phi^2 \right\rangle = \frac{\bar{\Phi}_T^2(h)}{\cos\theta} + \frac{\bar{\Phi}_v^2(h)}{\cos\theta}, \quad \left\langle \chi^2 \right\rangle \ll \left\langle \phi^2 \right\rangle; \quad (87)$$

$$D_{T,v} \gg 1: \quad \left\langle \phi^2 \right\rangle = \left\langle \chi^2 \right\rangle = \frac{\bar{\Phi}_T^2(h)}{2\cos\theta} + \frac{\bar{\Phi}_v^2(h)}{2\cos\theta}. \quad (88)$$

It follows from these formulas that the variances (except for $\left\langle \chi^2 \right\rangle$ for $D_{T,v} \ll 1$) are expressed in terms of the strength parameters $\bar{\Phi}_{T,v}^2(h) = 2h\bar{\gamma}_{T,v}^2(h)$. Therefore, the numerical results for $\bar{\gamma}_{T,v}^2(h)$ (Figs. 5 and 6) can be used to readily asses the variances.

For $D_{T,v} \sim 1$, numerical analysis of the correlation functions and variances for vertical and slanted propagation can be done similarly to Sections 3 and 4 and is not presented here for brevity.

6.3. Elevated sources

Now consider the case of an elevated source and ground-based receiver, which is important for correct formulations of signals propagating from flying aircraft. In previous work [16, 17], the correlation functions B_ϕ and B_χ were calculated without accounting for the height dependence of the variances and length scales of atmospheric turbulence, wind velocity fluctuations were ignored, and the temperature fluctuations were modeled using the Gaussian spectrum.

For the elevated source, the correlation functions B_ϕ and B_χ are given by Equation (77), where the integration is performed from the source ($l = 0$) to the ground-based receiver ($l = L$) and $\Phi_{\text{eff}} = \Phi_{\text{eff}}((L - l)\cos\theta; \kappa)$. Using manipulations similar to those above, it can be shown that B_ϕ and B_χ are still given by Equation (80), where the non-dimensional functions $\Psi_{T,v}$ are given by Equation (75) and the non-dimensional functions $\tilde{\Psi}_{T,v}$ are

$$\begin{aligned}\tilde{\Psi}_{T,v}(L, r) = &\int_0^1 \mathrm{d}\eta\, \mu_{T,v}(\eta, h) \int_0^\infty \hat{\Phi}_{T,v}(\eta h; \hat{\kappa}) \\ &\cdot J_0\left(\frac{(1-\eta)\hat{\kappa} r}{L_{T,v}(\eta h)}\right) \\ &\cdot \cos\left[\eta(1-\eta)\hat{\kappa}^2 D_{T,v}(L, \eta h)\right] \hat{\kappa}\, \mathrm{d}\hat{\kappa}.\end{aligned} \tag{89}$$

As for the MCF, this formula can be obtained from Equation (81) by replacing η with $1 - \eta$ in the argument of the Bessel function J_0.

For the considered case, the variances of the phase and log-amplitude fluctuations are given by Equation (86), where the non-dimensional functions $\tilde{\Psi}_{T,v}(L, 0)$ are determined with Equation (89).

7. Conclusions

A general theory of sound propagation though inhomogeneous turbulence [2] has been applied for the statistical characteristics of sound signals propagating over vertical and slanted paths in a turbulent atmosphere, in which the variances and length scales of temperature and wind velocity fluctuations depend on the height above the ground.

Formulations were provided for the extinction coefficient of the mean sound field, the strength parameter, the transverse MCF, the coherence radius, and the correlation functions and variances of the phase and log-amplitude fluctuations. These results were obtained for arbitrary turbulence spectra, and then specialized to the generalized von Kármán spectra. The contributions to the statistical characteristics of sound signals due to temperature fluctuations, shear-driven velocity fluctuations, and buoyancy-driven velocity fluctuations were identified and analyzed. Two geometries were considered: (i) a source on the ground and an elevated receiver, and (ii) an elevated source and a receiver on the ground. The extinction coefficient and coherence radius were calculated for the von Kármán spectra and different meteorological regimes of the atmospheric boundary layer characterized by the surface heat flux and friction velocity. The results obtained were compared with those for horizontal propagation.

The extinction coefficient for slanted propagation was found to coincide with that for vertical propagation. It is equal to the height-averaged extinction coefficient for horizontal propagation and is the same for the two considered geometries. For the sound frequency $f = 1\,\text{kHz}$ and the receiver height $h = 200\,\text{m}$, the extinction coefficient varies from $6 \times 10^{-3}\,\text{m}^{-1}$ to about $1\,\text{m}^{-1}$ for different meteorological conditions of the atmospheric boundary layer. The extinction coefficient for the receiver height h is approximately equal to that for horizontal propagation at the height $z = h/2$ above the ground.

The strength parameters for vertical and slanted propagation were calculated. It was shown that the strength parameter and the extinction coefficient are interchangeable. Therefore, most of the results obtained for the extinction coefficient are also applicable for the strength parameter.

The transverse MCF of the sound field was calculated and expressed in terms of the strength parameters for temperature and wind velocity fluctuations and the non-dimensional functions $\Psi_{T,v}(h, r)$, which characterize the dependence of the MCF on the sensor separation r. The MCF for a slanted path differs from that for a vertical path only by the factor $1/\cos\theta$ in the exponential, where θ is the propagation angle. The MCFs for the two considered geometries do not coincide; i.e., the reciprocity is not valid. For the ground-based source, the receiver height $h = 200\,\text{m}$, and the sound frequency $f = 1\,\text{kHz}$, the coherence radius varies from 5 m to more than 50 m for different meteorological conditions. For the elevated source, the coherence radius can differ by a factor 1.5 from that for the ground-based source.

Other statistical characteristics of sound signals propagating over vertical and slanted paths in a turbulent atmosphere, such as the variance of the angle-of-arrival fluctuations and the travel time and form of a pulse, can be calculated similarly. As an example of such calculations, formulations for the spatial correlation functions and variances of the phase and log-amplitude fluctuations of acoustic signals were outlined. The temporal mutual coherence function and temporal correlation functions of the phase and log-amplitude fluctuations are readily obtained if, in Equations (57) and (80), the sensor separation r is replaced with $v_\perp t$, where t is time and $v_\perp$ is the wind velocity component perpendicular to the sound propagation path. This substitution is valid for frozen turbulence and height-independent wind velocity. If the velocity depends on height, similarly to the variances and length scales of turbulence in Equations (57) and (80), $v_\perp$ might be replaced with $v_\perp(\eta h)$. To rigorously verify this substitution, an analysis should be done similar to that in [24]; this analysis is beyond the scope of the current paper.

Currently there are no experimental data to which the theoretical results obtained can be usefully compared. The theoretical results in this article will be used for determining geometries, frequencies, and signal forms for an experiment involving vertical and slanted sound propagation. Plans are underway to conduct such an experiment with the ground-based source and microphones located at different heights on a 135-m meteorological tower.

Acknowledgment

This research was sponsored by the U.S. Army Engineer Research and Development Center, Geospatial Research and Engineering business area. Permission to publish was granted by the Director, Cold Regions Research and Engineering Laboratory.

References

[1] K. Attenborough, K. M. Li, K. Horoshenkov: Predicting Outdoor Sound. Taylor and Francis, London, 2006, 441 pp.

[2] V. E. Ostashev and D. K. Wilson: Acoustics in Moving Inhomogeneous Media, Second Edition. CRC Press, Boca Raton, FL, 2015, 521 pp.

[3] V. E. Ostashev, D. K. Wilson, S. L. Collier, J. Cain, S. Cheinet: Cross-frequency coherence and pulse propagation in a turbulent atmosphere. J. Acoust. Soc. Am. **140**(1) (2016) 678–691.

[4] P. H. Parkin, W. E. Scholes: Air-to-ground sound propagation. J. Acoust. Soc. Am. **26**(6) (1954) 1021–1023.

[5] P. H. Parkin, W. E. Scholes: Oblique air-to-ground sound propagation over buildings. Acustica **8**(2) (1958) 99–102.

[6] M. Aubry, F. Baudin, A. Weill, P. Rainteau: Measurement of the total attenuation of acoustic waves in the turbulent atmosphere. J. Geophys. Res. **79**(36) (1974) 2156–2202.

[7] P. K. Kasper, R. S. Pappa, L. R. Keefe, L. C. Sutherland: A Study of Air-to-Ground Sound Propagation Using an Instrumented Meteorological Tower, NASA CR 2617. NASA, Washington, D.C., 1975.

[8] M. A. Johnson, R. Raspet, M. T. Bobak: A turbulence model for sound propagation from an elevated source above level ground. J. Acoust. Soc. Am. **81**(3) (1987) 638–646.

[9] H. E. Bass, L. N. Bolen, R. Raspet, W. McBride, J. Noble: Acoustic propagation through a turbulent atmosphere: Experimental characterization. J. Acoust. Soc. Am. **90**(6) (1991) 3307–3313.

[10] P. D. Schomer and M. J. White: A statistical description of sound propagation: A comparison of elevated and near-ground sources. Noise Control Eng. J. **54**(3) (2006) 157-168.

[11] D. Maglieri, P. Bobbitt, K. Plotkin, K. Shepherd, P. Coen, D. Richwine: Sonic Boom: Six Decades of Research. NASA/SP-2015-622. NASA, Washington, D.C., 2014.

[12] P. Boulanger, R. Raspet, H. E. Bass: Sonic boom propagation through a realistic turbulent atmosphere. J. Acoust. Soc. Am. **98**(6) (1995) 3412–3417.

[13] T. A. Stout and V. Sparrow: Statistics of supersonic signatures propagated through simulated atmospheric turbulence. J. Acoust. Soc. Am. **141**(5) (2017) Pt. 2, 3729.

[14] Ph. Blanc-Benon, B. Lipkens, L. L. Dallois, M. F. Hamilton, D. T. Blackstock: Propagation of finite amplitude sound through turbulence: Modeling with geometrical acoustics and the parabolic approximation. J. Acoust. Soc. Am. **111** (2002) 487–498.

[15] F. Coulouvrat, D. Luquet, R. Marchiano: Numerical model of sonic boom in 3D kinematic turbulence. AIP Conference Proceedings 1685, 090008 2015. https://doi.org/10.1063/1.4934474.

[16] F. Rietdijk, J. Forssén, K. Heutschi: Generating sequences of acoustic scintillations. Acta Acust united Ac **103**, (2017) 331–338.

[17] A. R. Aumann, S. A. Rizzi: An atmospheric turbulence model pugin for the NASA auralization framework. J. Acoust. Soc. Am. **141**(5) (2017) Pt. 2, 3885–3886.

[18] V. E. Ostashev and D. K. Wilson: Strength and wave parameters for sound propagation in random media. J. Acoust. Soc. Am. **141**(3) (2017) 2079–2092.

[19] V. E. Ostashev and D. K. Wilson: Erratum: Strength and wave parameters for sound propagation in random media [J. Acoust. Soc. Am. **141**(3) (2017) 2079–2092]. J. Acoust. Soc. Am. **143**(4) (2018) 2164.

[20] D. K. Wilson, V. E. Ostashev, G. H. Goedecke: Sound-wave coherence in atmospheric turbulence with intrinsic and global intermittency. J. Acoust. Soc. Am. **124**(2) (2008) 743–757.

[21] I. Toselli, L. C. Andrews, R. L. Phillips, V. Ferrero: Free-space optical system performance for laser beam propagation through non-Kolmogorov turbulence. Opt. Eng. **47**(2) (2008) 026003–026009.

[22] B. Xue, L. Cui, W. Xue, X. Bai, F. Zhou: Generalized modified atmospheric spectral model for optical wave propagating through non-Kolmogorov turbulence. J. Opt. Soc. Am. A **28**(5) (2011) 912.

[23] H. G. E. Hentschel and I. Procaccia: Passive scalar fluctuatations in intermittent turbulence with applications to wave propagation. Phys. Rev. A **28** (1983) 417–426.

[24] V. E. Ostashev, D. K. Wilson, S. N. Vecherin, S. L. Collier: Spatial-temporal coherence of acoustic signals propagating in a refractive, turbulent atmosphere. J. Acoust. Soc. Am. **136**(5) (2014) 2414–2431.